
VOLUME 26, ISSUE 5, SEPTEMBER-OCTOBER 2007
ISSN 0997-7538
ELSEVIER
EUROPEAN JOURNAL OF MECHANICS
Editor in chief
Viggo Tvergaard, Lyngby (Denmark)
Associate Editors
A. Benallal, Cachan (France)
A. Corigliano, Milano (Italy)
P. Eberhard, Stuttgart (Germany)
N.A. Fleck, Cambridge (UK)
J.-B. Leblond, Paris (France)
E. van der Giessen, Groningen (The Netherlands)
(Founded in 1961 as Journal de Mécanique)
A/SOLIDS

Available online at www.sciencedirect.com
ScienceDirect
ELSEVIER
European Journal of Mechanics A/Solids 26 (2007) 837–853

Distributed piezoelectric actuation of a bistable buckled beam

Corrado Maurini [a,*], Joël Pouget [a], Stefano Vidoli [b]

[a] *Institut Jean Le Rond d'Alembert, CNRS (UMR 7190), Université Pierre et Marie Curie, 4, place Jussieu, 75252 Paris cedex 05, France*
[b] *Dipartimento di Ingegneria Strutturale e Geotecnica, Università di Roma La Sapienza, via Eudossiana 18, 00184, Rome, Italy*

Received 22 August 2006; accepted 14 February 2007

Available online 14 March 2007

Abstract

Bistable structures, such as buckled beams or plates, are characterized by a two-well potential. Their nonlinear properties are currently exploited in actuators design (e.g. MEMS micropumps, switches, memory cells) to produce relatively high displacements and forces with low actuation energies. We investigate the use of distributed multiparameter actuation to control the buckling and postbuckling behavior of a three-layer piezoelectric beam pinned at either end. A two-parameter bending actuation controls the transversal motion, whilst an axial actuation and a beam end-shortening modulate the tangent bending stiffness. The postbuckling behavior is studied by reducing to a 2 dof system a nonlinear extensible elastica model. When the bending actuation is spatially symmetric, the postbuckling phenomena are analogue to those obtained for a transversal midspan force, being characterized by a snap-through instability. The use of a two-parameter actuation opens new transition scenarios, where it is possible to get true quasi-static transitions between the two specular equilibria of the buckled beam, without any instability phenomenon. The efficiencies of these different transition paths are discussed in terms of energetic requirements and stability properties. A numerical example shows the technical feasibility of the proposed actuation technique.

Keywords: Bistable; Morphing structures; Snap-through; Actuators; Extensible elastica

1. Introduction

The use of active materials for shape control of flexible structures has received a great attention for advanced technologies. The design of precise surfaces for antenna reflectors in communication satellites or the active control of airplane wings and helicopter rotor blades (Loewy, 1997) are among the specific applications in aeronautical and astronautical engineering. In the fields of micro-electromechanical systems, applied and fundamental research works investigated the production of micro-actuators and micro-motors (Qiu et al., 2004; Ren and Gerhard, 1997; Schomburg and Goll, 1998; Kueppers et al., 2002).

Available active materials include piezoelectric ceramics, shape memory alloys, electroactive polymers, and magnetostrictive materials. They can impose desired local strains or reduce vibrations for dynamic control (Sun and Tong, 2002; Batra and Geng, 2001; Alessandroni et al., 2005). Among the cited smart materials, piezoelectric ceramics are the most popular. This is mainly due to the linearity of their response for a large frequency bandwidth. Nevertheless,

* Corresponding author. Tel.: +33 (0)1 44275484; fax: +33 (0)1 44275259.
E-mail addresses: maurini@lmm.jussieu.fr (C. Maurini), pouget@lmm.jussieu.fr (J. Pouget), stefano.vidoli@uniroma1.it (S. Vidoli).

0997-7538/$ – see front matter
doi:10.1016/j.euromechsol.2007.02.001

piezoelectric materials produce limited displacements and strains. Efforts to overcome this drawback comprise a smart structural design, where the materials components and the geometry are optimized to enhance the action of the active elements (Frecker, 2003; Schwartz and Narayanan, 2002).

An efficient solution to produce high displacements with moderate actuation efforts is the use of bistable structures, such as buckled beams or shallow arches. These structures are characterized by two (or more) stable equilibrium configurations. The role of the actuator is limited to trigger the transition between the different equilibria; by instability phenomena, a rather small amount of actuating energy can induce relatively high displacements. This concept is quite popular in the design of MEMS devices which exploit the snap-through of curved beams (Vangbo, 1998; Qiu et al., 2004; Ren and Gerhard, 1997; Schomburg and Goll, 1998; Saif, 2000) or arches (Hsu, 1967; Chen and Lin, 2005) with transverse midspan loading. Similarly, Schultz and Hyer (2003) investigated the use of piezoelectric actuation for inducing snap-through of bistable composite plates with thermal pre-stresses.

To the authors' knowledge, the current literature on bistable structures considers only a single parameter actuation, given, for beam and plates, by either a piezoelectric voltage or a transverse force. When the actuating parameter reaches its critical value, the system becomes unstable and dynamically snaps toward a new stable equilibrium. This transition through a dynamic buckling is advantageous for systems such as relays, switches, and memory cells requiring a fast snap with a low actuation energy. Other applications (e.g. shape control, micromirrors, valves, etc.) require a precise control of the system configuration all along the transition path between the stable equilibria, which is impossible with a single parameter actuation under force or voltage control.

The aim of the present paper is to investigate the transition scenarios opened by a distributed multiparameter actuation of a bistable structure. In particular, we will show that suitably driving several distributed actuators introduces the possibility of smooth quasi-static transitions between two stable equilibria and allows for the reduction of the voltage requirements. To this end, we consider a straight sandwich three-layer piezoelectric beam pinned at either end (Section 2). This apparently simple system has a particularly rich nonlinear behavior which can be exploited for actuator design. An extensional actuating voltage and the end-shortening play the role of buckling parameters (de Faria, 2004), whilst two bending actuation voltages control the transverse motion and the transition between the equilibria of the buckled beam.

Despite the many past and current works on buckling and postbuckling of elastic beams (Antman, 1995; Bazant and Cedolin, 1991; Thompson and Hunt, 1973; Quoc Son, 1995; Dym, 1974), the development of a reliable nonlinear structural model for the buckling and postbuckling analyses of a pinned-pinned elastic beam with induced piezoelectric actuation is a delicate task. The standard approaches take the beam axis displacements as kinematical descriptors and apply approximated strains measures for the bending and extensional deformations (Qiu et al., 2004; Vangbo, 1998; Chen and Lin, 2005; Lacarbonara et al., 2004). In this paper (Section 3), we adopt an extensible elastica model (Magnusson et al., 2001; Coffin and Bloom, 1999; Stemple, 1990), where the beam kinematics is described in terms of the cross-sectional rotations only. The material behavior is assumed to be linear and the piezoelectric effect is modeled by extensional and flexural induced strains, which are evaluated by using an equivalent single layer beam theory (Crawley and Anderson, 1990; Maurini et al., 2004). This approach, being based on a single-field formulation, renders the derivation of asymptotic approximations straightforward and rigorous in the hypothesis of small rotations. The model is derived on the basis of a Lagrangian formulation, which is directly applied to stability analysis. The postbuckling scenarios are investigated by a reduced order model (Rega and Troger, 2005) obtained as a linear combination of the first two buckling modes.

By applying the stability theory for finite-dimensional potential systems (Thompson and Hunt, 1973; Huseyin, 1986), we discuss the effect of the axial (Section 4) and bending (Section 5) actuations on the main buckling and postbuckling phenomena (as snap-through, limit point, and branching instability). The geometric properties of the beam energy functional show that unstable configurations lie inside bounded regions of the configuration space. By considering a two-parameter bending actuation, different transition paths between the two stable equilibria of the buckled beam are investigated. Their efficiency is compared in terms of stability properties and energetic requirements. The technical feasibility of the proposed actuation technique is proved by a numerical example (Section 6). The paper concludes by discussing the main results and the possible extensions of the present work (Section 7).

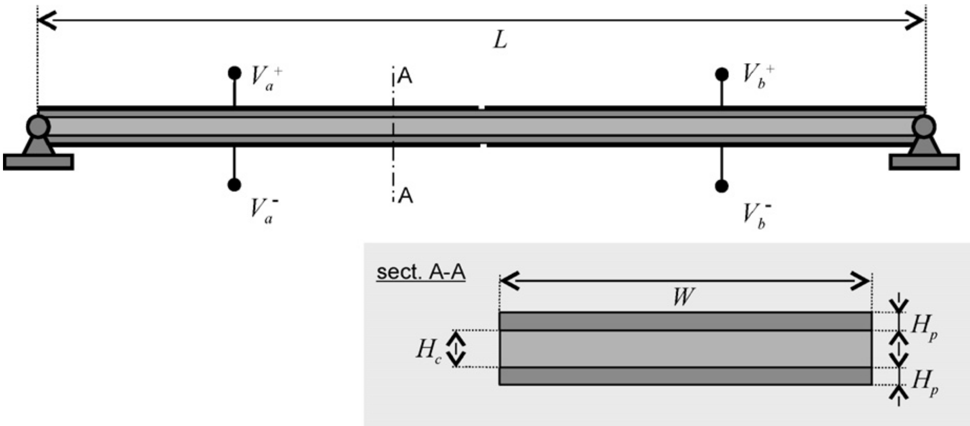

Fig. 1. Sandwich beam and piezoelectric patches. The beam section is drawn with the main dimensions.

2. Description of the system

We consider a simply supported sandwich piezoelectric beam of length L and width W; it is composed of two identical external piezoelectric layers (thickness H_p) bonded on an elastic core (thickness H_c). The beam is subjected to an end-shortening $\bar{w}$ that reduces the distance between the pin-joints. For each piezoelectric layer, the internal surface (e.g. the surface towards the elastic layer) is covered by a grounded electrode, whilst the external surface has two distinct electrodes of equal length, as shown in Fig. 1. Hence, from the electric point of view, four control voltages are available: the potentials (V_a^+, V_b^+) and (V_a^-, V_b^-) of the upper and lower electrodes of the left part (a) and the right part (b). Both piezoelectric layers are polarized along the thickness, but in opposite directions. The voltages are parameterized by the following nondimensional quantities:

$$\eta_\oplus = \frac{V_a^+ + V_a^- + V_b^+ + V_b^-}{4\,V_\eta}, \qquad \eta_\ominus = \frac{V_a^+ + V_a^- - V_b^+ - V_b^-}{4\,V_\eta}, \tag{1}$$

$$\delta_\oplus = \frac{V_a^+ - V_a^- + V_b^+ - V_b^-}{4\,V_\delta}, \qquad \delta_\ominus = \frac{V_a^+ - V_a^- - V_b^+ + V_b^-}{4\,V_\delta}, \tag{2}$$

that respectively control the symmetric $(\oplus)$ and skew-symmetric $(\ominus)$ parts of the extensional (η) and the bending actuation (δ), where V_η and V_δ are corresponding scaling voltages.

In the following, the end-shortening and the extensional actuation will play the role of buckling parameters. Once their values are fixed, we exploit the distributed bending actuation to introduce a transversal deflection in prebuckled beams and to switch between different equilibria in postbuckled beams.

3. Modelling

3.1. Nonlinear kinematics of a planar unshearable beam

The described set-up is modeled as a purely extensible and flexible beam undergoing in-plane deformations (Antman, 1995). The beam reference configuration $\mathcal{C}_0$ is assumed to be the straight line:

$$\mathcal{C}_0 = \{q_0(s) = s e_1,\ s \in [0, L]\},$$

where s is the abscissa and q_0 is the position vector in the Cartesian reference frame $\{o, e_1, e_2\}$. The actual configuration of the beam is a smooth curve (see Fig. 2)

$$\mathcal{C} = \{q(s) = q_0(s) + w(s)e_1 + v(s)e_2,\ s \in [0, L]\},$$

where q is the current position vector and the fields w and v respectively mean the displacements along the coordinate directions. Let $\theta(s)$ be the angle between the tangent to $\mathcal{C}$ in $q(s)$ and the e_1 direction; then the unit tangent and normal vectors to $\mathcal{C}$ in $q(s)$ are

$$\begin{cases} t(s) = \cos\theta(s)e_1 + \sin\theta(s)e_2, \\ n(s) = -\sin\theta(s)e_1 + \cos\theta(s)e_2, \end{cases} \tag{3}$$

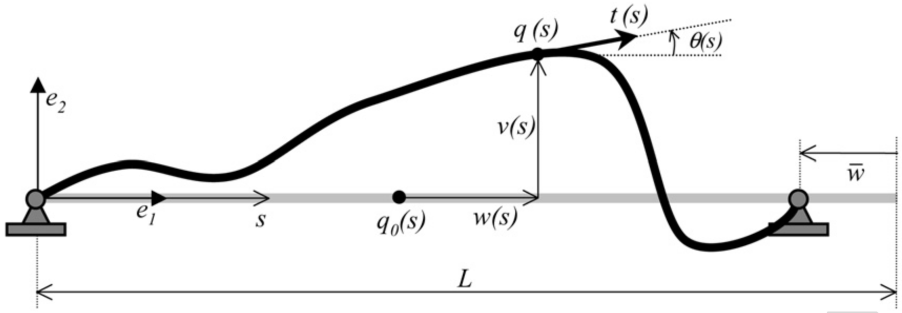

Fig. 2. Kinematical descriptors for the beam model and considered reference frame.

with

$$\tan\theta(s) = \frac{v'(s)}{1+w'(s)}. \tag{4}$$

The extensional strain $\varepsilon(s)$ and the beam curvature $\chi(s)$ are chosen as the two strain measures. They are defined by:

$$\varepsilon(s) := q'(s)\cdot t(s) - 1 = \frac{1+w'(s)}{\cos\theta(s)} - 1, \qquad \chi(s) := t'(s)\cdot n(s) = \theta'(s). \tag{5}$$

3.2. Nonlinear Lagrangian formulation

The strain measures (5) are the visible (or geometric) deformations of a nonlinear unshearable beam. The elastic energy per unit line $\mathcal{E}(s)$ is assumed to be a quadratic form of the two strain measures ε and χ:

$$\mathcal{E}(s) = \frac{1}{2}B(s)\big(\chi(s) - \bar{\chi}(s)\big)^2 + \frac{1}{2}A(s)\big(\varepsilon(s) - \bar{\varepsilon}(s)\big)^2, \tag{6}$$

where $A(s)$ and $B(s)$ are, respectively, the extensional and bending stiffnesses of the sandwich beam. The strains $\bar{\varepsilon}(s)$ and $\bar{\chi}(s)$ can be interpreted as the strains in a natural (stress-free) configuration. Here, they model the piezoelectrically induced deformations, being constitutively related to the applied voltages on the piezoelectric electrodes. For the sandwich beam in Fig. 1, the piezoelectrically induced strains are given by

$$\bar{\varepsilon}(s) = qV_\eta(\eta_\oplus \pm \eta_\ominus), \qquad \bar{\chi}(s) = pV_\delta(\delta_\oplus \pm \delta_\ominus), \tag{7}$$

where the plus sign is for $s \leqslant L/2$ and the minus sign is for $s > L/2$. The constants p and q are the extensional and bending piezoelectric couplings, respectively. Equivalent single-layer beam models of piezoelectric laminates (Crawley and Anderson, 1990; Maurini et al., 2004) give the expressions of A, B, p, q for specific cross-sectional geometry and material properties of the piezoelectric beam.

By choosing the horizontal displacement $w(s)$ and the angle $\theta(s)$ as kinematical descriptors, the energy functional for quasi-static regimes (or Lagrangian) is defined as follows:

$$\mathcal{L}(w',\theta,\theta') = \int_0^L \mathcal{E}(s)\,\mathrm{d}s = \frac{1}{2}\int_0^L \left[B(s)\big(\theta'(s) - \bar{\chi}(s)\big)^2 + A(s)\left(\frac{1+w'(s)}{\cos\theta(s)} - 1 - \bar{\varepsilon}(s)\right)^2\right]\mathrm{d}s. \tag{8}$$

The associated Euler–Lagrange equations are:

$$\frac{N(s)}{\cos\theta(s)} = C, \qquad M'(s) - \big(1+w'(s)\big)\tan\theta(s)\,\frac{N(s)}{\cos\theta(s)} = 0, \tag{9}$$

with the boundary conditions:

$$\big[C\,\delta w(s)\big]_0^L = 0, \qquad \big[M(s)\delta\theta(s)\big]_0^L = 0, \tag{10}$$

where:

$$N(s) = \frac{\partial\mathcal{L}}{\partial\varepsilon} = A(s)\big(\varepsilon(s) - \bar{\varepsilon}(s)\big), \qquad M(s) = \frac{\partial\mathcal{L}}{\partial\chi} = B(s)\big(\chi(s) - \bar{\chi}(s)\big), \tag{11}$$

are the extensional force (or tension) and the bending moment, respectively. The Lagrangian does not depend on the variable w, and Eq. $(9)_1$ represents the corresponding first integral ($\partial\mathcal{L}/\partial w' = C$). Its constant value C represents the horizontal (along e_1), statically undetermined, reaction. For a simply supported beam the geometrical boundary conditions are $w(0) = 0$, $w(L) = -\bar{w}$, whilst, since the rotations at the pins are free, Eq. $(10)_2$ imposes that $M(0) = M(L) = 0$. The substitution of Eq. $(11)_1$ in Eq. $(9)_1$ and the definition of the extensional strain $(5)_1$ give:

$$w'(s) = \frac{C\cos^2\theta(s)}{A(s)} + \big(1 + \bar{\varepsilon}(s)\big)\cos\theta(s) - 1. \tag{12}$$

Hence, integrating Eq. (12) on the beam length and using the boundary conditions on w, leads to the following expression for the statically undetermined horizontal reaction C as a function of the configuration θ, of the extensional actuation $\bar{\varepsilon}$, and of the end-shortening $\bar{w}$:

$$C(\theta, \bar{\varepsilon}, \bar{w}) = \frac{L - \bar{w} - \int_0^L (1 + \bar{\varepsilon}(s))\cos\theta(s)\,\mathrm{d}s}{\int_0^L (\cos^2\theta(s)/A(s))\,\mathrm{d}s}. \tag{13}$$

Eqs. (12), (13) allow for the elimination of the variable w' from the Lagrangian (8). Thus the problem is formulated in terms of the rotation field θ by using the energy functional:

$$\mathcal{L}\big(\theta, \theta'\big) = \frac{1}{2}\int_0^L B(s)\big(\theta'(s) - \bar{\chi}(s)\big)^2\,\mathrm{d}s + \frac{C^2(\theta, \bar{\varepsilon}, \bar{w})}{2}\int_0^L \frac{\cos^2\theta(s)}{A(s)}\,\mathrm{d}s. \tag{14}$$

The corresponding nonlinear Euler–Lagrange is computed to get:

$$\big[B(s)\big(\theta'(s) - \bar{\chi}(s)\big)\big]' - C(\theta, \bar{\varepsilon}, \bar{w})\big(1 + \bar{\varepsilon}(s)\big)\sin\theta(s) - \frac{C^2(\theta, \bar{\varepsilon}, \bar{w})}{A(s)}\cos\theta(s)\sin\theta(s) = 0, \tag{15}$$

with the boundary conditions still determined by Eq. $(10)_2$.

Remark 1. The Lagrangian (14) gives the exact energy functional of the geometrically fully nonlinear theory of a simply supported unshearable beam, accounting for both extensional and bending deformations. With respect to other approaches based on the choice of the horizontal and vertical displacements as kinematical descriptors (Lacarbonara et al., 2004), the present extensible elastica model has the advantage of providing a relatively simple description of the exact Lagrangian on the basis of a single field, the cross-sectional rotation. This simplifies the formulation of rigorous asymptotic expansions of the energy functional.

Remark 2. The Lagrangian (8) does not account for the boundary conditions on the vertical displacement v; these constraints can be considered augmenting the Lagrangian with a suitable Lagrange multiplier:

$$\mathcal{L}_{\mathrm{aug}} = \mathcal{L} + \mu(v_L - v_0) = \mathcal{L} + \mu\int_0^L \big(1 + w'(s)\big)\tan\theta(s)\,\mathrm{d}s. \tag{16}$$

For the present case of a simply supported beam with no external loads, Eqs. (9) show that

$$v_L - v_0 = \int_0^L \big(1 + w'(s)\big)\tan\theta(s)\,\mathrm{d}s = \frac{1}{C}\int_0^L M'(s)\,\mathrm{d}s = \frac{1}{C}\big(M(L) - M(0)\big) = 0; \tag{17}$$

Thus, the boundary conditions on the vertical displacement are automatically satisfied and $\mathcal{L}_{\mathrm{aug}} \equiv \mathcal{L}$.

3.3. Approximations and dimensional analysis

The formulation in terms of a single field, the rotation $\theta(s)$, allows for the straightforward development of coherent approximations of the fully nonlinear theory based on the extensible elastica model. In the following, we introduce the nondimensional variables

$$\tilde{\mathcal{L}} := \frac{\mathcal{L}}{A_0 L}, \quad \xi := \frac{s}{L}, \quad \tilde{A}(\xi) := \frac{A(\xi L)}{A_0}, \quad \tilde{B}(\xi) := \frac{B(\xi L)}{B_0} = \frac{1}{\beta}\frac{\pi^2 B(\xi L)}{A_0 L^2}, \tag{18}$$

where:

$$A_0 := \frac{L}{\int_0^L (1/A(s))\,\mathrm{d}s}, \qquad \beta := \pi^2\left(\frac{R}{L}\right)^2. \tag{19}$$

The nondimensional parameter β is inversely proportional to the square of the beam slenderness, $R := \sqrt{B_0/A_0}$ being the radius of gyration of the cross-section. Physically, β represents the *beam extensibility* and is the key parameter for buckling and postbuckling analysis.

By assuming that the rotations are small, the nonlinear terms of the energy functional can be expanded as a power series of θ. By including the terms up to the fourth order we find:

$$\tilde{\mathcal{L}}(\theta,\theta') \simeq \frac{\beta}{2\pi^2}\int_0^1 \tilde{B}(\xi)\left(\frac{\mathrm{d}\theta(\xi)}{\mathrm{d}\xi} - L\bar{\chi}(\xi)\right)^2 \mathrm{d}\xi + \tilde{\mathcal{L}}_2(\theta) + \tilde{\mathcal{L}}_4(\theta), \tag{20}$$

with:

$$\tilde{\mathcal{L}}_2(\theta) := -\frac{1}{2}\bar{\varepsilon}_m\int_0^1 \left(1 + \bar{\varepsilon}(\xi) - \frac{1}{\tilde{A}(\xi)}\bar{\varepsilon}_m\right)\theta(\xi)^2\,\mathrm{d}\xi,$$

$$\tilde{\mathcal{L}}_4(\theta) := \frac{1}{8}\left(\int_0^1 \left(1 + \bar{\varepsilon}(\xi) - 2\frac{1}{\tilde{A}(\xi)}\bar{\varepsilon}_m\right)\theta(\xi)^2\,\mathrm{d}\xi\right)^2 + \frac{1}{24}\bar{\varepsilon}_m\int_0^1 \left(1 + \bar{\varepsilon}(\xi) - \frac{4}{\tilde{A}(\xi)}\bar{\varepsilon}_m\right)\theta(\xi)^4\,\mathrm{d}\xi. \tag{21}$$

Here the parameter

$$\bar{\varepsilon}_m := \frac{1}{L}\int_0^L \bar{\varepsilon}(s)\,\mathrm{d}s + \frac{\bar{w}}{L} = q V_\eta \eta_\oplus + \frac{\bar{w}_0}{L}\omega \tag{22}$$

is an average induced extensional strain. The latter expression introduced the nondimensional end-shortening ω and the associated scaling displacement $\bar{w}_0$.

Buckling takes place when the linearized stiffness vanishes. This means that the flexural energy associated with the first terms on the r.h.s. of Eq. (20) and the quadratic term $\tilde{\mathcal{L}}_2(\theta)$ must be of the same order of magnitude. This is obtained if $\bar{\varepsilon}_m \sim \beta$. Moreover in early postbuckling, buckled beams reach the equilibrium when the quartic term $\tilde{\mathcal{L}}_4(\theta)$ of the Lagrangian counterbalances the quadratic contributions. This happens for $\theta \sim \sqrt{\beta}$. In view of Eqs. (7), (20), and (22), in order to meet these conditions with nondimensional variables of the order of the unity, we set

$$\bar{w}_0 = \beta L, \quad V_\eta = \frac{\beta}{q}, \quad V_\delta = \frac{\sqrt{\beta}}{pL}. \tag{23}$$

3.4. Buckling: eigensolution of the linearized problem

For the simply-supported beam with vanishing bending actuation, the trivial equilibrium configuration $\theta(s) = 0$ satisfies Eq. (15). But there are critical values for the induced axial deformation $\bar{\varepsilon}(s)$ and for the end-shortening $\bar{w}$ leading to the appearance of solutions with $\theta(s) \neq 0$. These critical values are associated to the eigenvalues of the linearized version of the equilibrium equation around $\theta(s) = 0$. The Euler–Lagrange equations of the second-order Lagrangian obtained by Eq. (20) with $\tilde{\mathcal{L}}_4 = 0$, read

$$\frac{\mathrm{d}}{\mathrm{d}\xi}\left[\tilde{B}(\xi)\frac{\mathrm{d}\theta(\xi)}{\mathrm{d}\xi}\right] + \pi^2\lambda(\xi)\theta(\xi) = 0, \qquad \left.\frac{\mathrm{d}\theta}{\mathrm{d}\xi}\right|_0 = \left.\frac{\mathrm{d}\theta}{\mathrm{d}\xi}\right|_1 = 0, \tag{24}$$

where

$$\lambda(\xi) := \frac{\bar{\varepsilon}_m}{\beta}\left(1 + \bar{\varepsilon}(\xi) - \frac{\bar{\varepsilon}_m}{\tilde{A}(\xi)}\right), \tag{25}$$

is the *Effective Buckling Parameter* (EBP).

For the constant cross-section beam, such as the one drawn in Fig. 1, with a constant axial actuation ($\eta_\ominus = 0$, $\eta_\oplus = \eta$), the eigenvalue problem (24) is solved in closed form; indeed $A(x) = A_0$, $B(x) = B_0$ and $\tilde{A}(\xi) = \tilde{B}(\xi) = 1$. The EBP (25) becomes

$$\lambda(\xi) = \lambda = (\eta + \omega)(1 - \beta\omega). \tag{26}$$

Its critical values and the corresponding buckling modes are

$$\lambda^{(j)} = j^2, \quad \theta^{(j)}(\xi) = c_j \cos j\pi\xi, \quad j = 1, 2, \ldots, \tag{27}$$

where the c_j's are arbitrary normalization constants.

Eq. (26) shows that in the present extensible elastica model the axial actuation and the end-shortening play different roles in the EBP. The axial actuation is equivalent to the hygrothermal buckling studied by Coffin and Bloom (1999), whilst the end-shortening is equivalent to the case of an applied end-force analyzed by Magnusson et al. (2001) and Stemple (1990). In the exact extensible elastica beam theory, the quadratic dependence of λ on the end-shortening causes nonstandard effects, such as finite number of buckling modes and double bifurcations (Magnusson et al., 2001). Herein we assume the hypothesis of a slender beam ($\beta \ll 1$) for which

$$\lambda \simeq (\eta + \omega). \tag{28}$$

This leads us to ignore the difference between the role of the end-shortening and the role of the axial actuation as buckling parameters. For the sake of simplicity, we study the postbuckling behavior as a function of the axial actuation η by setting $\omega = 0$. Nevertheless, in the case of slender beams, similar buckling and postbuckling phenomena can be obtained also by imposing an equivalent end-displacement ω or a combination of η and ω.

3.5. *Hypotheses and methods for the nonlinear analysis*

3.5.1. *Finite-dimensional approximation*

We study the beam postbuckling behavior under the hypothesis of moderate rotations $\theta(s)$ by using the approximated fourth-order expansion of the energy functional given in Eq. (20). Moreover, in order to get a qualitative outlook of the effect of distributed multiparameter actuation, we take a *finite-dimensional approximation* of the system by expanding the state field $\theta(s)$ in truncated series of buckling modes (Rega and Troger, 2005):

$$\theta(\xi) \simeq \hat{\theta}(\xi) = \sum_{j=1}^{J} \Theta_j \theta^{(j)}(\xi), \quad \Theta := \{\Theta_j,\ j = 1, 2, \ldots, J\} \in \mathbb{R}^J. \tag{29}$$

The corresponding finite-dimensional fourth-order Lagrangian appears in the form

$$\hat{\mathcal{L}}(\Theta; \delta_\oplus, \delta_\ominus, \eta, \omega) = \frac{1}{2}\big(K_{ij}^{(0)} - S_{ij}(\eta, \omega)\big)\Theta_i\Theta_j + F_{ijlm}(\eta, \omega)\Theta_i\Theta_j\Theta_l\Theta_m + \delta_\oplus A_{\oplus,i}\Theta_i + \delta_\ominus A_{\ominus,i}\Theta_i, \tag{30}$$

where the expressions for the matrices ($K_{ij}^{(0)}$, $S_{ij}(\eta, \omega)$, $F_{ijlm}(\eta, \omega)$) and the vectors ($A_{\oplus,i}$, $A_{\ominus,i}$) are given in Appendix A. Implicit summation on repeated indices is used.

The Galerkin expansion (29) including J buckling modes is justified for the postbuckling analysis if the EBP λ ranges below $\lambda^{(J+1)}$. For moderate rotations, this condition implies a convex dependence of the Lagrangian on the coefficients $\Theta_{j>J}$ of the higher order modes. This means that the configurations with $\Theta_{j>J} = 0$ are stable with respect to $\Theta_{j>J}$ and prevents the beam from instabilities on the coordinates $\Theta_{j>J}$. Here and henceforth, the analysis is made in the hypothesis of moderate rotations for which the modal expansion with $J = 2$ holds at least for $\lambda < \lambda^{(3)}$. Thus we assume a two d.o.f. model by setting:

$$\theta(\xi) = \Theta_1 \sqrt{12\beta}\cos(\pi\xi) + \Theta_2\, 2\sqrt{12\beta}\cos(2\pi\xi). \tag{31}$$

The corresponding expression for the fourth-order energy functional is computed to be

$$\hat{\mathcal{L}}(\Theta_1, \Theta_2; \delta_\oplus, \delta_\ominus, \eta, \omega) = 4\sqrt{3}(\delta_\oplus\Theta_1 + 4\delta_\ominus\Theta_2) + a_1\Theta_1^2 + 4a_2\Theta_2^2 + b_1\big(\Theta_1^4 + 16\Theta_2^4\big) + 4b_2\Theta_1^2\Theta_2^2, \tag{32}$$

where

$$\begin{aligned} a_1 &= 3\big(1 - \eta - \omega\big(1 - \beta(\eta + \omega)\big)\big), & b_1 &= \frac{9}{4}\big(2 - \beta(3\eta + 7\omega) - \beta^2\big(\eta^2 - \omega(\eta + 4\omega)\big)\big), \\ a_2 &= 3\big(4 - \eta - \omega\big(1 - \beta(\eta + \omega)\big)\big), & b_2 &= 9\big(1 - \beta\,\eta - 2\beta^2\eta^2 - 3\beta\omega(1 + \beta\eta)\big). \end{aligned} \tag{33}$$

3.5.2. Equilibria and stability

The equilibrium configurations are defined as the solutions of

$$\frac{\partial \hat{\mathcal{L}}}{\partial \Theta_i} = \big(K_{ij}^{(0)} - S_{ij}(\eta,\omega)\big)\Theta_j + 4F_{ijlm}(\eta,\omega)\Theta_j\Theta_l\Theta_m + \delta_\oplus A_{\oplus,i} + \delta_\ominus A_{\ominus,i} = 0, \tag{34}$$

with $i = 1,\ldots,J$ and implicit summation on j,l,m. Their stability is studied by using the Dirichlet theorem for potential systems (Thompson and Hunt, 1973; Huseyin, 1986; Quoc Son, 1995; Kounadis et al., 2004). the $J \times J$ Hessian matrix of $\hat{\mathcal{L}}$ is

$$H_{ij}(\Theta;\eta,\omega) = \frac{\partial^2 \hat{\mathcal{L}}(\Theta;\delta,\eta,\omega)}{\partial\Theta_i\partial\Theta_j} = K_{ij}^{(0)} - S_{ij}(\eta,\omega) + 12F_{ijlm}(\eta,\omega)\Theta_l\Theta_m. \tag{35}$$

If H is positive definite, i.e. if all the eigenvalues of H are positive, the system is stable because the energy functional is convex. If one or more eigenvalues are negative the system is unstable, because the energy functional is concave in one or two directions determined by the associated eigenspaces.

4. Effect of the axial actuation

The axial actuation η modifies the nonlinear terms of the energy functional and influences the stability properties. We focus our analysis on the behavior of the beam for symmetric axial actuation ($\eta_\ominus = 0$, $\eta_\oplus = \eta$) such that

$$0 < \lambda = \eta < \lambda^{(3)} = 9. \tag{36}$$

For the EBP within this range, the two d.o.f. model of Eqs. (31), (32) holds.

4.1. Pre- and post-buckling scenarios

The bifurcation diagram of Fig. 3 displays the equilibrium configurations of the system as a function of the buckling parameter λ for vanishing bending actuation ($\delta_\oplus = \delta_\ominus = 0$). This follows the classical pitchfork bifurcation diagram (Antman, 1995; Bazant and Cedolin, 1991; Quoc Son, 1995) and shows three different scenarios, depending on the value of the EBP:

(a) $\lambda < \lambda^{(1)}$: there is a single, stable, equilibrium point, $\Theta^I = 0$. The lower plane of Fig. 3 reports the associated contour plot of the Lagrangian.

(b) $\lambda^{(1)} < \lambda < \lambda^{(2)}$: there are three equilibrium points, namely:

$$\Theta^{\mathrm{I}} = 0, \quad \Theta^{\mathrm{II}}_\pm = \{\pm\Theta^{\mathrm{II}}(\lambda), 0\}; \tag{37}$$

where $\Theta^{\mathrm{II}}_\pm$ are stable minima, whilst Θ^{I} is an unstable maximum. The middle plane of Fig. 3 displays the corresponding contour plot of the Lagrangian.

(c) $\lambda^{(2)} < \lambda < \lambda^{(3)}$: there are five equilibrium points, namely:

$$\Theta^{\mathrm{I}} = 0, \quad \Theta^{\mathrm{II}}_\pm = \{\pm\Theta^{\mathrm{II}}(\lambda), 0\}, \quad \Theta^{\mathrm{III}}_\pm = \{0, \pm\Theta^{\mathrm{III}}(\lambda)\}; \tag{38}$$

where $\Theta^{\mathrm{II}}_\pm$ are stable minima, Θ^{I} is an unstable maximum, and $\Theta^{\mathrm{III}}_\pm$ are unstable saddles points. The characteristic contour plot of the Lagrangian is drawn in the upper plane.

The equilibrium Θ^{I} corresponds to the rectilinear configuration of the beam with a purely compressive axial strain depending on λ. The equilibria $\Theta^{\mathrm{II}}_\pm$ and $\Theta^{\mathrm{III}}_\pm$ correspond to buckled configurations on the first and second buckling modes. For relatively slender beam, by neglecting higher order terms in β,we find

$$\Theta^{\mathrm{II}}(\lambda) \simeq \sqrt{\frac{\lambda-1}{3}}, \qquad \Theta^{\mathrm{III}}(\lambda) \simeq \frac{1}{2}\sqrt{\frac{\lambda-4}{3}}. \tag{39}$$

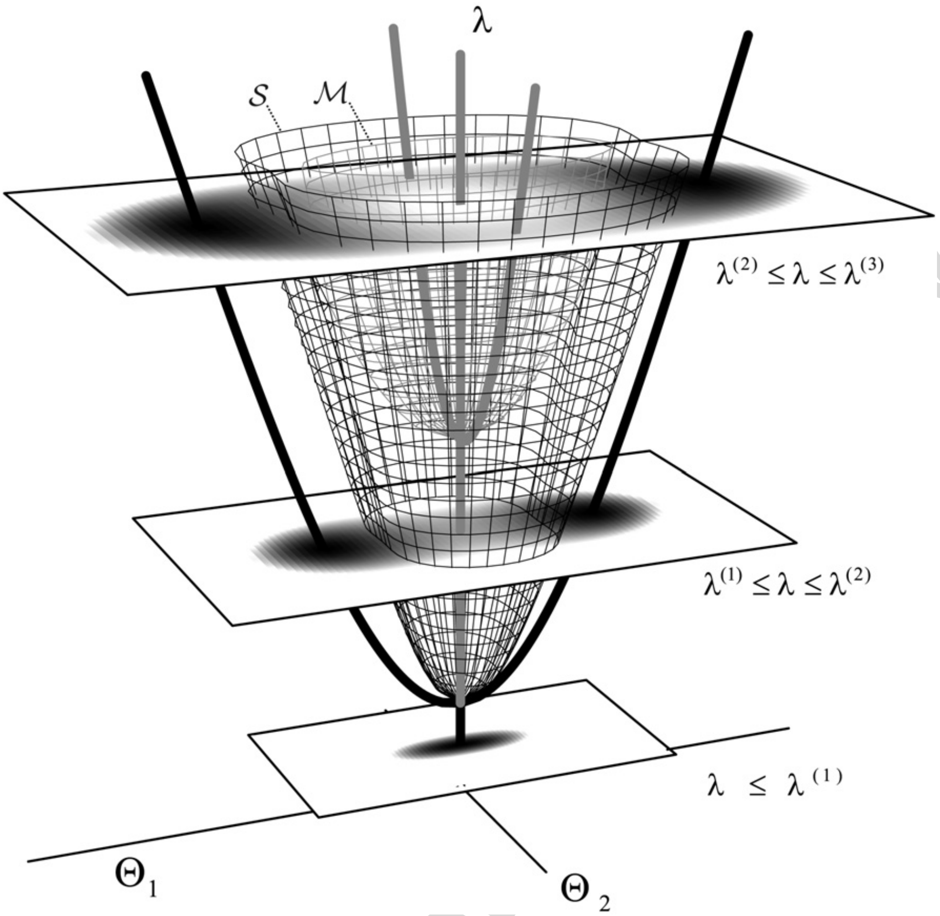

Fig. 3. Bifurcation diagram for the two-dimensional approximation of the system as a function of the EBP. Stable equilibrium paths are in black, whilst gray denotes unstable equilibria. The grids $\mathcal{S}$ and $\mathcal{M}$ bound the instability regions. The planes show the typical contour plots of the Lagrangian.

4.2. Stability regions

The meshed surfaces $\mathcal{S}$ and $\mathcal{M}$ of Fig. 3 represent, as a function of λ, the configurations for which at least one of the eigenvalue of the 2×2 Hessian matrix (35) is equal to zero. These surfaces partition the $(\Theta - \lambda)$ space in three regions:

1. The region external to $\mathcal{S}$ where both eigenvalues of H are positive. Here, the energy functional is convex and the equilibrium configurations inside this region are stable minima.
2. The region between $\mathcal{S}$ and $\mathcal{M}$ where the Hessian matrix H has one positive eigenvalue and one negative eigenvalue. In this region, the energy functional is concave along the eigenspace associated to negative eigenvalue and convex in the orthogonal direction. All the equilibria are unstable saddles.
3. The region inside $\mathcal{M}$ where the Hessian matrix H has two negative eigenvalues. Here, the energy functional is concave and the equilibria are unstable maxima.

The intersections between the $\mathcal{S}$ and $\mathcal{M}$ surfaces and the Θ_1 and Θ_2 axes are computed to get $(\beta \ll 1)$:

$$\Theta_1\text{-axis}: \quad \Theta_1^{\mathcal{S}}(\lambda) \simeq \pm\frac{1}{3}\sqrt{\lambda - 1}, \qquad \Theta_1^{\mathcal{M}} \simeq \pm\sqrt{\frac{(\lambda - 4)}{3}}, \tag{40}$$

$$\Theta_2\text{-axis}: \quad \Theta_2^{\mathcal{S}}(\lambda) \simeq \pm\frac{1}{2}\sqrt{\frac{\lambda - 1}{3}}, \qquad \Theta_2^{\mathcal{M}} \simeq \pm\frac{1}{6}\sqrt{(\lambda - 4)}. \tag{41}$$

For

$$\lambda = \lambda^{(c)} = \frac{11}{2}, \tag{42}$$

the surfaces $\mathcal{S}$ and $\mathcal{M}$ intersect on the Θ_1-axis at the abscissae $\pm\Theta_1^{(c)} \simeq 1/\sqrt{2}$. In these points, both the eigenvalues of H vanish; the quadratic part of the energy functional $\hat{\mathcal{L}}$ is degenerate and higher order terms determine the stability properties (Thompson and Hunt, 1973; Huseyin, 1986).

Remark 3. For small rotations, the midspan vertical displacement v_m along the stable equilibrium paths $\Theta_\pm^{\mathrm{II}}(\lambda)$ of the buckled beam is approximated by

$$v_m(\lambda) \simeq \int_0^{L/2} \theta(s)\,\mathrm{d}s = \pm\, 2\sqrt{3}\,\frac{L\sqrt{\beta}}{\pi}\,\Theta_\pm^{\mathrm{II}}(\lambda) \simeq \pm 2R\sqrt{\lambda - 1}. \tag{43}$$

5. Effect of the distributed bending actuation

The bending actuation including both the symmetric ($\delta_\oplus$) and skew-symmetric ($\delta_\ominus$) contributions is equivalent to a generalized force having two independent components on the Θ_1 and Θ_2 variables. These forces modify the equilibria of the system. An arbitrary position $\bar{\Theta}$ becomes an equilibrium when applying the actuation obtained by solving for $\delta_\oplus$ and $\delta_\ominus$ the system (34) with $\Theta = \bar{\Theta}$. However, the Hessian matrix (35) is independent of δ. Thus, the stability of any equilibrium $\bar{\Theta}$ is independent of the bending actuation (this is true also for the infinite-dimensional Lagrangian (8)). Referring to Fig. 3, the equilibrium paths are deformed, but the stability surfaces are unchanged.

5.1. Actuation for $\lambda < \lambda^{(1)}$

For $\lambda < \lambda^{(1)}$ the beam is always stable. The local stiffness at the origin is controlled by the EBP λ. The linear model is valid only for $\lambda \ll 1$. When λ approaches the critical strain $\lambda^{(1)} = 1$ the local stiffness vanishes and the system behavior is controlled by the nonlinear effects. For $\lambda \to 1$ the quartic terms of the energy functional (30) become the leading contributions. Within this framework, the extensional piezoelectric actuation can be used to adjust the bending stiffness by varying λ. This has two possible applications: (i) to increase the stiffness and to enhance the buckling limit for the end-shortening $\bar{w}$ (buckling enhancement, e.g. de Faria (2004)); (ii) to decrease the stiffness for increasing the midspan displacement for a fixed bending actuation.

5.2. Actuation for $\lambda^{(1)} < \lambda < \lambda^{(2)}$

For $\lambda > \lambda^{(1)}$ the structure becomes bistable with a bounded instability region around the origin limited by $\mathcal{S}$. The bending actuation is used to induce a transition between the stable equilibrium points Θ_-^{II} to Θ_+^{II}, and vice-versa. This transition results in a midspan displacement, with the further advantage that the system maintains the deformed shape without the need of continued actuation.

Fig. 4 shows a contourplot of the Lagrangian for $\delta_\ominus = \delta_\oplus = 0$ and $\lambda^{(1)} < \lambda < \lambda^{(2)}$. The white solid line is the trace of the surface $\mathcal{S}$ and marks the limit of the instability region. The bending actuation will add to the energy functional a plane passing through the origin. As already discussed, this modifies the positions of the equilibria but leaves invariant the instability region. Hence, the transition between the two equilibria Θ_-^{II} and Θ_+^{II} can be obtained by choosing the bending actuation according to two qualitatively different transition paths:

- the equilibrium path (o) on the Θ_1-axis passing through the instability region;
- the equilibrium path (s), which is an elliptic path between Θ_-^{II} and Θ_+^{II} circumventing the instability region.

The equilibrium path (o) corresponds to the standard snap-through phenomenon of shallow arches (Bazant and Cedolin, 1991; Dym, 1974). Moving the equilibrium configuration along this path (with a displacement-controlled mechanism) requires the purely symmetric actuation voltage ($\delta_\oplus$) shown in Fig. 5. In a voltage-controlled actuation

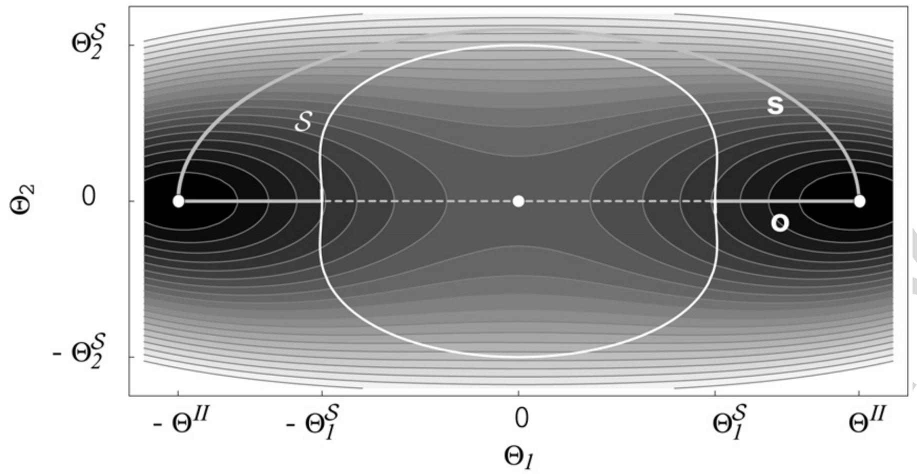

Fig. 4. Contourplot of the Lagrangian for $\lambda^{(1)} < \lambda < \lambda^{(2)}$ on the plane $\{\Theta_1, \Theta_2\}$ for vanishing bending actuation. White points correspond to equilibria; the instability region is bounded by the solid white curve $\mathcal{S}$. It is possible to choose the bending actuation to move the equilibria along two different kinds of paths crossing and circumventing $\mathcal{S}$, respectively labeled as "o" and "s".

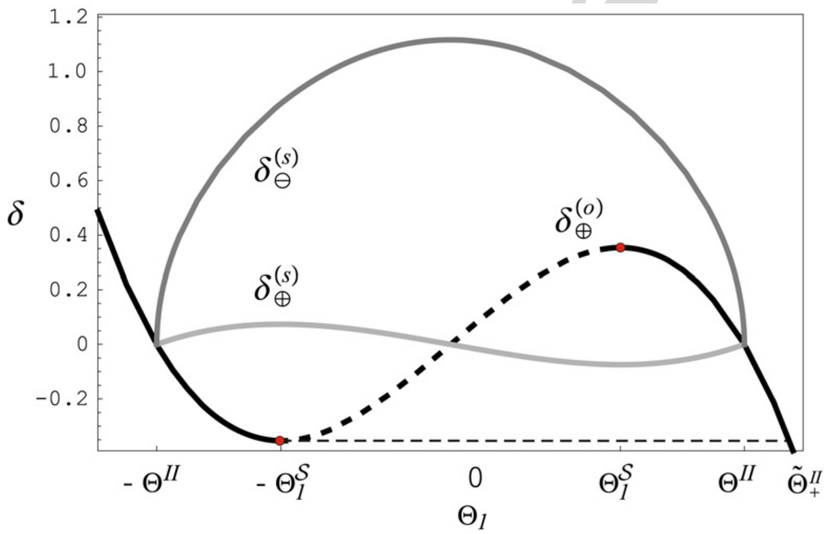

Fig. 5. Bending actuation needed to follow the paths "o" (black) and "s" (gray). In the latter case two curves are drawn for the symmetric and skewsymmetric parts of the actuation voltages. The plot is for $\lambda = 2.5$.

it is possible to quasi-statically move along the path (o) only until the point $\Theta_-^{\mathcal{S}}$, intersection with the instability region, is reached. At this point the system becomes unstable on the symmetric mode (Θ_1-direction) and jumps to the position $\tilde{\Theta}_+^{\mathrm{II}}$ which is the only possible stable equilibrium. In this stage the process is dynamic, with the system starting (damped, in real systems) oscillations around $\tilde{\Theta}_+^{\mathrm{II}}$. Hence, when decreasing the voltage to zero, the equilibrium position moves quasi-statically along the $\tilde{\Theta}_+^{\mathrm{II}}$–$\Theta_+^{\mathrm{II}}$. Now, for $\delta = 0$ the system stays in Θ_+^{II}.

The equilibrium path (s) is made of *stable equilibrium points* and can be fully covered quasi-statically with a voltage-control. The required actuation is made both by symmetric ($\delta_\oplus$) and skew-symmetric components ($\delta_\ominus$), as reported in Fig. 5. The maximum required voltage to pass from the two stable equilibrium point Θ_-^{II} to Θ_+^{II} is higher than the voltage required by the (o) path. However, the (s) path avoids instability phenomena and allows for a true quasi-static transition with a voltage control. At the best of our knowledge, this is the first paper discussing this stable transition path between two configurations of a buckled beam.

Remark 4. The standard consideration that the system is stable when the force-displacement relation has a positive slope is valid only for the rectilinear path (o), for which $\delta_\ominus = 0$ and the loading is controlled by the single parame-

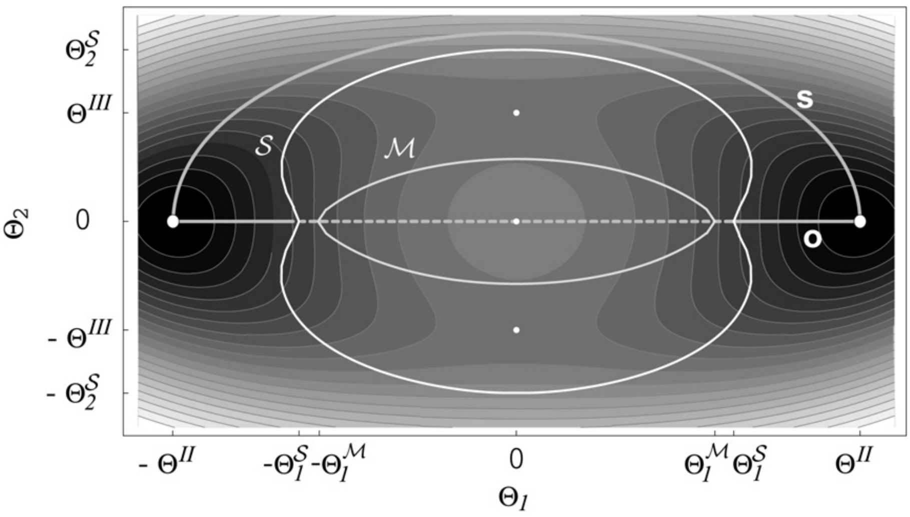

Fig. 6. Contourplot of the Lagrangian for $\lambda^{(2)} < \lambda < \lambda^{(3)}$ on the plane $\{\Theta_1, \Theta_2\}$ for vanishing bending actuation.

ter $\delta_\oplus$. Here the only criterion used for stability is the curvature of the energy functional, being the defined in terms of the eigenvalues of H.

5.3. *Actuation for* $\lambda^{(2)} < \lambda < \lambda^{(3)}$

For $\lambda^{(2)} < \lambda < \lambda^{(3)}$ there are the two additional equilibrium points $\Theta_\pm^{\mathrm{III}}$ shown in Fig. 6. They are saddle points lying inside the instability region. The behavior of the system on the (s) path is qualitatively similar to the previous case of $\lambda^{(1)} < \lambda < \lambda^{(2)}$. This path is always made of stable equilibria and allows the system for a quasi-static transition between the two buckled states Θ_-^{II} and Θ_+^{II}. On the other hand, when moving the equilibria Θ_-^{II} (or Θ_+^{II}) towards the origin on the (o) path by a purely symmetric actuation ($\delta_\oplus = \delta,\ \delta_\ominus = 0$), the system shows a different behavior. Indeed, for $\lambda > \lambda^{(2)}$ the equilibrium path on the Θ_1-axis has a branching on the second mode; depending on the value of λ, the instability will take place either on the symmetric or the skew-symmetric mode. The two cases are distinguished by the value of the effective strain $\lambda^{(c)} = 11/2$ for which the two instability surfaces in Fig. 3 intersect on the Θ_1-axis (see Eqs. (40)–(42)):

- For $\lambda^{(2)} < \lambda < \lambda^{(c)} = 11/2$ the instability is activated on the first mode, because the intersection between the (o) path and the instability surface $\mathcal{S}$ is associated to a limit point instability along the Θ_1-direction. Fig. 7 shows the corresponding equilibrium paths in the Θ_1–Θ_2 plane as a function of $\delta_\oplus = \delta$. When the equilibrium path intersects the second instability surface $\mathcal{M}$, there is a branching on the second mode. In a dynamic process, the beam starts snapping on a purely symmetric shape but it will not pass through the straight configuration. When the configuration will cross $\mathcal{M}$, a skew-symmetric contribution to the beam deflection will appear and the beam will snap through an asymmetric configuration.
- For $\lambda^{(c)} < \lambda < \lambda^{(3)}$ the instability is activated on the second mode, because the intersection between the (o) path and the instability surface $\mathcal{S}$ is associated with a supercritical pitchfork bifurcation with the branching on the second mode. Fig. 8 reports the associated equilibrium paths, where the branching on the second mode takes place before the limit point of the fundamental equilibrium path. In this case, the beam will start snapping through a skew-symmetric shape.

Analog instability phenomena are well-known for shallow arches (Bazant and Cedolin, 1991; Quoc Son, 1995; Dym, 1974; Vannucci et al., 1998), where the switching between the symmetric snap at the limit-point and the asymmetric snap at the bifurcation on the second buckling mode depends on the arch height. For a pinned sine arch under end-couples, Chen and Lin (2005) predicted a critical value of the arch height for distinguishing between the two cases equal to $6.55R$. The critical value $\lambda^{(c)} = 11/2$, corresponds to a sine shaped buckled beam of height $v_m(\lambda^{(c)}) = 3\sqrt{2}R \simeq 4.24R$ (see Eq. (43)). The difference between these two values is not surprising because the systems are different: the sine-arches analyzed in Chen and Lin (2005), Vangbo (1998), Qiu et al. (2004) are stress-free

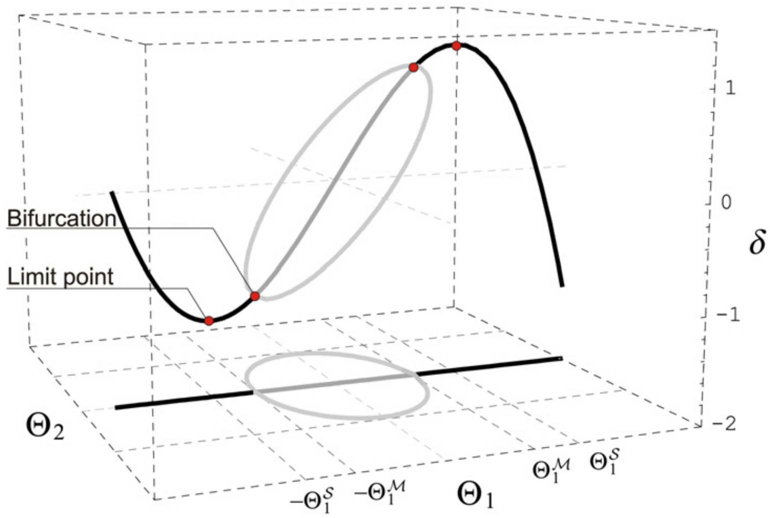

Fig. 7. Equilibrium paths for the beam under symmetric bending actuation ($\delta_\ominus = 0$) for $\lambda^{(2)} < \lambda < \lambda^{(c)} = 11/2$. Stable configurations are in black, unstable configurations in gray. The subcritical pitchfork bifurcation on the second mode follows the limit point instability on the first mode.

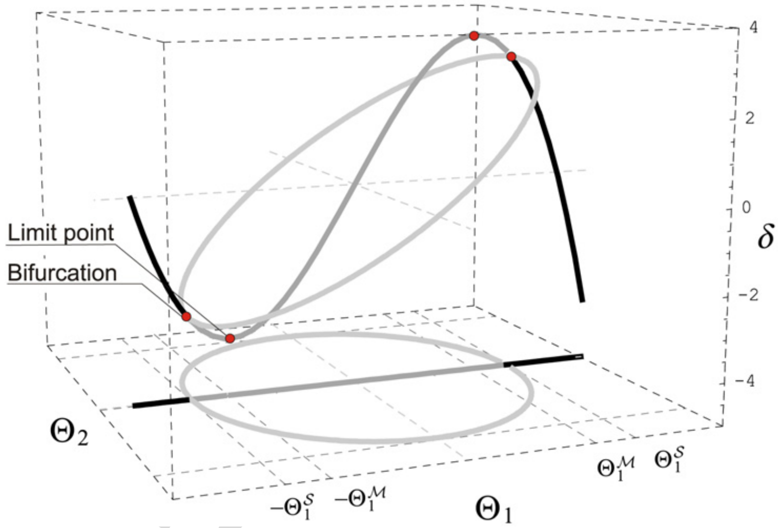

Fig. 8. Equilibrium paths for the beam under symmetric bending actuation ($\delta_\ominus = 0$) for $11/2 = \lambda^{(c)} < \lambda < \lambda^{(3)}$. The subcritical pitchfork bifurcation on the second mode precedes the limit point instability on the first mode.

in their reference configuration, whilst here the buckled beam has an initial axial prestress. In any case, the results are not directly comparable because the theories presented herein and in Chen and Lin (2005) are based on different approximations: our result is based on a two-mode approximation of the fourth-order functional (20), whilst the result of Chen and Lin (2005) includes the effect of all modes but adopts a simpler beam theory.

5.4. *Midspan displacement versus actuation energy*

The energy required to obtain a given midspan displacement characterizes the effectiveness of the simply-supported sandwich beam when used as an actuator. Fig. 9 compares the displacements obtainable in pre- and post-buckling regimes.

For $\lambda < \lambda^{(1)}$, the midspan displacement is achieved by moving the equilibrium configuration Θ^{I} through the generalized force exerted by the applied voltages. The dashed curves (1–3) in Fig. 9 show the energy-displacement curves for $\lambda = 0$, $\lambda = 0.5\lambda^{(1)}$ and $\lambda = 0.9\lambda^{(1)}$.

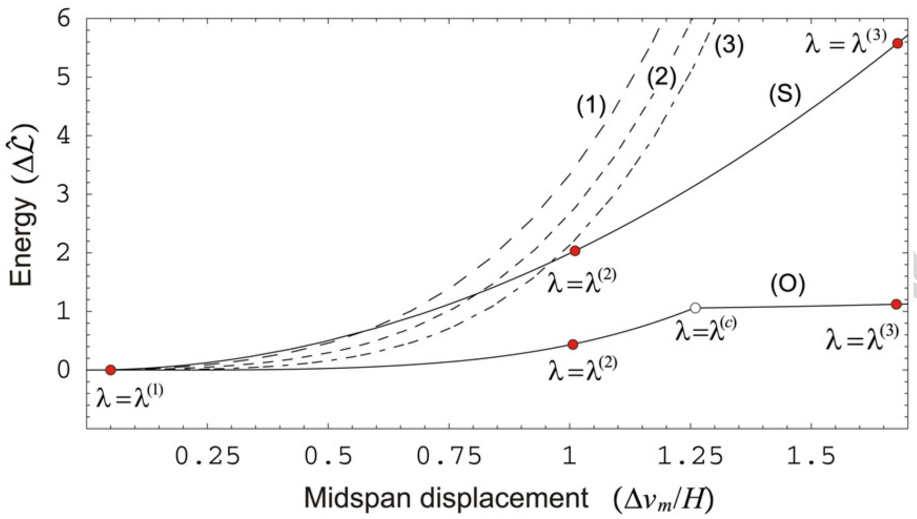

Fig. 9. Midspan displacements Δv_m versus bending actuation energies $\Delta\hat{\mathcal{L}}$ in pre- and post-buckling actuation techniques. The dashed curves are before buckling and for fixed values of the EBP, namely: $\lambda = 0$ (1), $\lambda = 0.5\lambda^{(1)}$ (2), and $\lambda = 0.9\lambda^{(1)}$ (3). The (o) and (s) solid curves are for the buckled bistable beams and are parameterized with the EBP for $\lambda^{(1)} < \lambda < \lambda^{(3)}$. In the latter case the midspan displacement is obtained by following either the (o) path or the (s) path. The reported actuation energy is the maximum of the actuation energy along (s) and the energy required to activate the snap-through instability along (o), respectively.

For $\lambda > \lambda^{(1)}$ the displacement is the result of the transition between the two symmetric equilibria Θ_-^{II} to Θ_+^{II}. For instance, for $\lambda = \lambda^{(2)} = 4$ the transition between Θ_-^{II} and Θ_+^{II} will result into the midspan displacement (see Eq. (43))

$$\Delta v_m = 2\left|v_m(\lambda = 4)\right| \simeq 2\sqrt{12}\,R \simeq 2H, \tag{44}$$

where H is the total height of the beam and the radius of gyration R is approximated by that one of a homogeneous rectangular cross-section ($R = H/\sqrt{12}$). This transition can be obtained by following either the equilibrium path (o) associated to the snap-through phenomenon or the path (s) of stable equilibria. In the path (o) the required energy to get the transition is the energetic gap between the boundary of the instability region $\Theta_1^{\mathcal{S}}$ and the initial equilibrium position Θ_-^{II}. For the transition with the stable path (s), the required energy is at least the difference between the energy at the point of $\Theta_2^{\mathcal{S}}$ and the energy at the initial state Θ_-^{II}. Fig. 9 reports these energy values as functions of the resulting midspan displacement, keeping λ as parameter. The angular point in the curve (o) corresponds to the critical EBP $\lambda^{(c)} = 11/2$, from which the instability is activated on the skew-symmetric mode. The comparison of the different curves leads to the following conclusions:

- Increasing λ under the first critical strain $\lambda^{(1)}$ increases the resulting displacement per applied energy. This is because λ modulates the linearized stiffness around $\Theta = 0$. For large displacements, this advantage is overridden by the stiffness contribution due to nonlinear effects.
- The snap-through phenomenon can be exploited to obtain large displacements with small amount of actuation energy. Especially, increasing λ beyond the critical value $\lambda^{(c)}$ for which the instability is activated on the second mode results in an increase of the resulting displacement without additional energy.
- The transition path (s) requires more energy than the path (o), but, for sufficiently high λ, less energy than the prebuckling actuation (curves 1–3).

6. Numerical example

The analysis of the previous sections is made in terms of nondimensional variables and shows that the transverse displacements of the buckled beam are of the same order of magnitude as the beam thickness. To get the numerical values of the voltages required to provoke beam buckling and the transition between the buckled states, we considered a realistic case study. Table 1 reports the corresponding material and geometric properties. The constitutive coefficients obtained for this configuration by adopting the beam model presented in Maurini et al. (2004) are reported in Appendix A. The cross-sectional radius of gyration is $R = 0.19$ mm and the beam extensibility is $\beta = 52.5 \times 10^{-6}$.

Table 1
Material and geometrical properties for the numerical case study

	PZT 5H	Aluminum
Length (L)	100 mm	100 mm
Width (W)	10 mm	10 mm
Thickness (H_p, H_c)	0.267 mm	0.267 mm
Young modulus (Y_{11}^E, Y)	62×10^9 Pa	69×10^9 Pa
Poisson ratio (ν_{12}^E, ν)	0.30	0.33
Strain constant (d_{31})	-320×10^{-12} m V^{-1}	–

Hence, by using the numerical values of Eq. (48), we find the following scaling voltages for the extensional and the bending actuation:

$$V_\eta = \frac{\beta}{q} = 68.7\ \mathrm{V}, \qquad V_\delta = \frac{\sqrt{\beta}}{pL} = 19.9\ \mathrm{V}. \tag{45}$$

These values and the nondimensional voltages in Figs. 5 and 7–8 show the technical feasibility of the proposed actuation technique of the simply-supported beam. In particular, for the considered geometry, the voltages required for the bending actuation in post-buckling regimes can be easily obtained in an experimental setup. Higher voltages are required for the axial actuation. This problem can be overcome by replacing the axial actuation with an equivalent end-shortening $\bar{w}$, which can be controlled through an external actuator, as proposed by Saif (2000).

The data reported in Table 1 refer to piezoelectric layers made of monolithic piezoelectric ceramics (PZT 5H, see e.g. www.piezo.com). For shape control applications, where high deformations are expected, these materials may prove too brittle. More appropriate would be the use of Macro Fiber Composite (MFC) layers made of piezoelectric fibers embedded in a soft matrix and covered by interdigitated electrodes (see e.g. Sodano et al., 2004). MFCs may experience much larger deformations before failure and currently appear the most suitable materials for shape control applications. In our case study, with the geometry specified in Table 1 and the typical values of the effective material constants of MFC ($Y_{11}^E = 30.34$ GPa, $d_{31} = -170 \times 10^{-12}$ m V^{-1} as specified for the P2-type MFC produced by Smart Materials GmbH, www.smart-materials.com) we found $V_\eta \simeq 130$ V, $V_\delta \simeq 31$ V. These numerical values show that, notwithstanding the reduced effective Young modulus and strain constants, MFC can exert the flexural actuation (V_δ) required by the proposed actuation technique with reasonable voltage values. The requirement of high voltages for the axial actuation is still a problem. This suggests, also in this case, the use of an external actuator for controlling the equivalent buckling parameter through an end-shortening.

7. Summary and concluding remarks

A nonlinear elastica theory is used for investigating the effect of distributed multiparameter actuation on a simply supported straight beam with end-shortening. After formulating a geometrically exact beam theory via a variational formulation based on a single state variable, namely the cross-sectional rotation, finite dimensional models for the buckling and postbuckling analysis were derived. The effect of the bending actuation on the bistable buckled beam was analyzed by a reduced order 2 d.o.f. model including the first two buckling modes. This simplified model allowed for a systematic analysis of the effect of the multiparameter actuation on the basis of the theory of stability for conservative finite dimensional systems, with the following results:

- The axial actuation plays the role of a buckling parameter. It can be used to modulate the linearized beam stiffness and to induce buckling. Its effect is similar (but in the nonlinear theory not identical) to that of an imposed end-shortening. The critical value of the axial actuation for inducing beam buckling depends on the beam extensibility, being proportional to the cross-sectional radius of gyration R. The corresponding postbuckling displacements are of the order of R and increase with the square root of the actuating voltage, as shown by Eq. (39).
- The stability of any configuration of the beam is independent of the bending actuation. Thus, bounded instability regions in the configuration space were characterized in terms of the axial actuation only.
- The multiparameter bending actuation allows for different types of transitions between the stable equilibrium points of the buckled beam. A purely symmetric bending actuation induces standard snap-through phenomena.

The first instability occurs either on the symmetric mode or on the skew-symmetric mode, depending on the value of the buckling parameter λ. When adding a skew-symmetric component to the bending actuation, the beam can switch between the two buckled configurations without any instability phenomenon. This is obtained by choosing the actuation voltages to follow an equilibrium path (s-path) which is entirely outside the instability region. This equilibrium path, characterized by a sequence of stable equilibria, can be of relevant interest for the engineering applications in which snap-through phenomena must be avoided.

The numerical example of Section 6 shows the technical feasibility and the effectiveness of the proposed actuation method. In particular, for a beam 10 cm long, displacements of the order of 1 mm can be obtained with about 100 V. On this basis, the manufacturing of demonstrative prototypes will be a natural extension of the present work. Moreover, it seems very promising to consider the use of multiparameter actuation in more complex structures such as deep arches, frames, and prestressed composite plates. From the modeling point of view, it remains to extend the present analysis to higher values of the buckling parameter, by including the effect of higher modes, and to investigate the effect of imperfections. To this end, the variational extensible elastica formulation seems particularly well-suited for nonlinear finite-element numerical implementations (Vannucci et al., 1998).

Acknowledgements

This work has been carried out in the framework of a joint research project between the University Pierre & Marie Curie and the University of Rome La Sapienza founded by the PAI-Galileo project #14383QD and the CNRS/CNR project #16283, which are gratefully acknowledged. Furthermore, we would like to thank Sébastien Neukirch and Adrien Mamou-Mani (Institut Jean Le Rond d'Alembert, Paris 6) for their stimulating discussions about the stability of elastic rods.

Appendix A. Energy functional for the finite dimensional model

The coefficients of the finite dimensional Lagrangian (30) are computed by substituting the expansion (29) in Eq. (20):

$$\begin{aligned}
&K_{ij}^{(0)} = \frac{\beta}{\pi^2} k_i \delta_{ij}, \qquad S_{ij}(\eta,\omega) = \beta(\eta+\omega)(1-\beta\omega)c_i\delta_{ij},\\
&F_{ijlm}(\eta,\omega) = \frac{(\beta(2\omega+\eta)-1)^2}{8} c_i c_l \delta_{ij}\delta_{lm} + \frac{\beta(\eta+\omega)(1-\beta(3\eta+4\omega))}{24} f_{ijlm},\\
&A_{\oplus,i} = -\frac{\beta\sqrt{\beta}}{\pi^2}\big(\theta^{(i)}(1)-\theta^{(i)}(0)\big), \qquad A_{\ominus,i} = -\frac{\beta\sqrt{\beta}}{\pi^2}\big(2\theta^{(i)}(1/2)-\theta^{(i)}(1)-\theta^{(i)}(0)\big),
\end{aligned} \tag{46}$$

where:

$$c_i := \int_0^1 \theta^{(i)}(\xi)^2\,\mathrm{d}\xi, \quad k_i := \int_0^1 \frac{\mathrm{d}\theta^{(i)}(\xi)}{\mathrm{d}\xi}^2\,\mathrm{d}\xi, \quad f_{ijlm} := \int_0^1 \theta^{(i)}(\xi)\theta^{(j)}(\xi)\theta^{(l)}(\xi)\theta^{(m)}(\xi)\,\mathrm{d}\xi, \tag{47}$$

and δ_{ij} is the Kronecker symbol. For the 2 d.o.f. model given by (29) and (31), the Lagrangian is given by Eqs. (32)–(33).

A.1. Piezoelectric constitutive equations

In an unshearable equivalent single-layer model, the linear constitutive equations for the sandwich beam in Fig. 1 are in the form specified by Eqs. (7) and (11). For the material and geometrical properties in Table 1, the beam model proposed in Maurini et al. (2004), which includes the effect of cross-sectional warping, provides the following numerical values for the constitutive coefficients

$$\begin{aligned}
&A_0 = 515\times 10^3\ \mathrm{N}, \qquad && B_0 = 27.4\times 10^{-3}\ \mathrm{N\,m^2},\\
&q = 0.762\times 10^{-6}\ \mathrm{V^{-1}}, && p = 3.64\times 10^{-3}\ \mathrm{m^{-1}\,V^{-1}}.
\end{aligned} \tag{48}$$

References

Alessandroni, S., Andreaus, U., dell'Isola, F., Porfiri, M., 2005. A passive electric controller for multimodal vibrations of thin plates. Computers and Structures 83, 1236–1250.

Antman, S.S., 1995. Nonlinear Problems of Elasticity. Springer-Verlag, New York.

Batra, R.C., Geng, T.S., 2001. Enhancement of the dynamic buckling load for a plate by using piezoelectric actuators. Smart Materials and Structures 10, 925–933.

Bazant, Z.P., Cedolin, L., 1991. Stability of Structures. Oxford University Press, New York.

Chen, J.S., Lin, J.S., 2005. Exact critical loads for a pinned half-sine arch under end couples. ASME Journal of Applied Mechanics 72, 147–148.

Coffin, D.W., Bloom, F., 1999. Elastica solution for the hygrothermal buckling of a beam. International Journal of Non-Linear Mechanics 34, 935–947.

Crawley, E.F., Anderson, E.H., 1990. Detailed models of piezoceramic actuation in beams. Journal of Intelligent Material Systems and Structures 1, 12–25.

de Faria, A.R., 2004. On buckling enhancement of laminated beams with piezoelectric actuators via stress stiffening. Composite Structures 65, 187–192.

Dym, C.L., 1974. Stability Theory and its Applications to Structural Mechanics. Noordhoff International Publishing Company, Leyden, The Netherlands. Republished by Dover in 2002.

Frecker, M.I., 2003. Recent advances in optimization of smart structures and actuators. Journal of Intelligent Material Systems and Structures 14, 207–216.

Hsu, C.S., 1967. The effects of various parameters on the dynamic stability of shallow arch. ASME Journal of Applied Mechanics 34, 349–358.

Huseyin, K., 1986. Multiple Parameter Stability Theory and its Applications. Oxford University Press, Oxford.

Kounadis, A.N., Gantes, C.J., Raftoyiannis, I.G., 2004. A geometric approach for establishing dynamics buckling loads of autonomous potential N-degree-of-freedom systems. International Journal of Non-Linear Mechanics 39, 1635–1646.

Kueppers, H., Leurerer, T., Schnakenberg, U., Mokwa, W., Hoffmann, M., Schneller, T., Boettger, U., Wase, R., 2002. Piezoelectric thin films for piezoelectric microactuator applications. Sensors and Actuators A 97–98, 680–684.

Lacarbonara, W., Paolone, A., Yabuno, H., 2004. Modeling of planar nonshallow prestressed beams towards asymptotic solutions. Mechanics Research Communications 31, 301–310.

Loewy, R.G., 1997. Recent developments in smart structures with aeronautical applications. Smart Materials and Structures 6, R11–R42.

Magnusson, A., Ristinmaa, M., Ljung, C., 2001. Behaviour of the extensible elastica solution. International Journal of Solids and Structures 38, 8441–8457.

Maurini, C., Pouget, J., dell'Isola, F., 2004. On a model of layered piezoelectric beams including transverse stress effect. International Journal of Solids and Structures 41, 4473–4502.

Qiu, J., Lang, J.H., Slocum, A.H., 2004. A curved-beam bistable mechanism. Journal of Microelectromechanical Systems 1, 137–146.

Quoc Son, N., 1995. Stabilité des Structures Elastiques. Springer-Verlag, Berlin.

Rega, G., Troger, H., 2005. Dimension reduction of dynamical systems: methods, models, applications. Nonlinear Dynamics 41, 1–15.

Ren, H., Gerhard, E., 1997. Design and fabrication of a current-pulse-excited bistable magnetic microactuator. Sensors and Actuators A: Physical 58, 259–264.

Saif, M.T.A., 2000. On a tunable bistable MEMS – Theory and experiment. Journal of Microelectromechanical Systems 9, 157–170.

Schomburg, W.K., Goll, C., 1998. Design optimization of bistable microdiaphragm valves. Sensors and Actuators A 64, 259–264.

Schultz, M.R., Hyer, M.W., 2003. Snap-through of unsymmetric cross-ply laminates using piezoceramic actuators. Journal of Intelligent Material Systems and Structures 14, 795–814.

Schwartz, R.W., Narayanan, M., 2002. Development of high performance stress-biased actuators through the incorporation of mechanical pre-loads. Sensors and Actuators A 101, 322–331.

Sodano, A.H., Park, G., Inman, D.J., 2004. An investigation into the performance of macro-fiber composites for sensing and structural vibration application. Mechanical System and Signal Processing 18, 683–697.

Stemple, T., 1990. Extensional beam-columns: an exact theory. International Journal of Non-Linear Mechanics 25, 615–623.

Sun, D., Tong, L., 2002. Static shape control of structures using nonlinear piezoelectric elements with energy constraints. Smart Materials and Structures 11, 163–168.

Thompson, J.M.T., Hunt, G.W., 1973. A General Theory of Elastic Stability. John Wiley & Sons, London.

Vangbo, M., 1998. An analytical analysis of a compressed bistable buckled beam. Sensors and Actuators A 69, 212–216.

Vannucci, P., Cochelin, B., Damil, N., Potier-Ferry, M., 1998. An asymptotic-numerical method to compute bifurcation branches. International Journal for Numerical Methods in Engineering 41, 1365–1389.